

Microsleeps are Associated with Stage-2 Sleep Spindles from Hippocampal-Temporal Network

Yaqub Jonmohamadi

*New Zealand Brain Research Institute
Christchurch, New Zealand*

*Department of Medicine, University of Otago
Christchurch, New Zealand*

*Department of Physics, University of Auckland
Auckland, New Zealand
y.jonmo@auckland.ac.nz*

Govinda R. Poudel

*New Zealand Brain Research Institute
Christchurch, New Zealand*

*Monash Biomedical Imaging, Monash University
Melbourne, Australia*

*School of Psychological Sciences, Monash University
Clayton, Victoria, Australia*

Carrie C. R. H. Innes

*New Zealand Brain Research Institute
Christchurch, New Zealand*

*Department of Electrical and Computer Engineering
University of Canterbury, Christchurch, New Zealand*

Richard D. Jones*

*New Zealand Brain Research Institute
Christchurch, New Zealand*

*Department of Medicine, University of Otago
Christchurch, New Zealand*

*Department of Electrical and Computer Engineering
University of Canterbury, Christchurch, New Zealand
richard.jones@canterbury.ac.nz*

Accepted 19 January 2016

Published Online 30 March 2016

Behavioral microsleeps are associated with complete disruption of responsiveness for ~ 0.5 s to 15 s. They can result in injury or death, especially in transport and military sectors. In this study, EEGs were obtained from five nonsleep-deprived healthy male subjects performing a 1 h 2D tracking task. Microsleeps were detected in all subjects. Microsleep-related activities in the EEG were detected, characterized, separated from eye closure-related activity, and, via source-space-independent component analysis and power analysis, the associated sources were localized in the brain. Microsleeps were often, but not always, found to be associated with strong alpha-band spindles originating bilaterally from the anterior

*Corresponding author.

temporal gyri and hippocampi. Similarly, theta-related activity was identified as originating bilaterally from the frontal-orbital cortex. The alpha spindles were similar to sleep spindles in terms of frequency, duration, and amplitude-profile, indicating that microsleeps are equivalent to brief instances of Stage-2 sleep.

Keywords: Beamformer; EEG; ICA; localization; microsleeps; sleep spindles; hippocampi; temporal lobes.

1. Introduction

Lapses in responsiveness ('lapses'), especially behavioral microsleeps ('microsleeps'), involve momentary (~0.5 to 15s) disruption of performance and can result in injury or death, especially in the transport sector (e.g. pilots, air-traffic controllers, truck, and car drivers, etc.). Microsleeps are characterized by full or partial eyelid closure, previous drowsy behavior, and absent task responsiveness.¹

1.1. EEG-based studies of microsleeps

Spectral analysis of EEG around microsleeps has shown an overall, but inconsistent, increase in EEG power in the delta (0–4 Hz), theta (4–8 Hz), and alpha (8–12 Hz) bands, and a decrease in EEG power in the beta (12–30 Hz) and gamma (> 30 Hz) bands.¹ Furthermore, EEG changes associated with microsleeps include alpha bursts^{2–6} and theta bursts.⁵

However, as most microsleeps are accompanied by eye closure, this raises the question: could the source of microsleep alpha be the same as that of voluntary eye closure alpha activity?

Little is known about the mechanisms in the brain underlying microsleeps. fMRI studies have provided spatial information on the origin of microsleep-related activities. They have shown that, during microsleeps, the BOLD signal (and, hence, neural activity) decreases bilaterally in the thalamus and posterior cingulate cortex but increases in several cortical brain regions, including the inferior frontal cortex, posterior parietal cortex, and occipital cortex.^{7,8} Furthermore, the extent of the decreases in neural activity in the thalamus increases with the duration of microsleeps.⁸ A study of functional connectivity during the transition to microsleeps found connectivity patterns involving left-right parietal and left-frontal right-parietal connection commencing 500 ms prior to the onset of microsleeps.⁹

A limitation in current EEG-based detection of microsleeps is that analysis is performed on sensor-space EEG data, where the source activities are highly overlapping and activity from one source in the brain is seen on all sensors. There is a recent trend of performing signal analysis (such as blind separation techniques or connectivity analysis) in the source-space (post inverse technique) rather than sensor-space.^{10–16} In source-space, the time courses of each brain location can be reconstructed and interference from neighboring sources minimized.

Several approaches have been proposed for solving the inverse problem, including dipole fitting,^{17–19} minimum-norm spatial filters,^{20–22} and minimum-variance spatial filters.^{23–28} Each approach has its advantages and disadvantages. A common limitation of inverse techniques is that they struggle to detect multiple concurrent sources. To overcome this latter limitation, mathematical approaches such as independent component analysis (ICA) and principal component analysis (PCA) can be applied in conjunction to provide an estimate of the active sources during an epoch of EEG. ICA is a blind source separation technique which aims to separate P mutually statistically independent, zero mean, sources from M linearly combined signal mixtures.²⁹ In EEG and MEG, ICA has been used for component extraction of event-related potentials (ERPs) and for artefact removal. Examples of applying ICA to help solve the inverse problem are ICA + dipole fitting³⁰ and ICA + sLORETA,³¹ both which applied ICA to sensor-space EEG. Recently, we proposed source-space ICA which applies ICA and PCA in source-space after minimum-variance beamforming.¹² This approach was shown to be superior to beamforming alone or sensor-space ICA in terms of spatial resolution and accuracy and detection of weak sources.

In this study, we have applied source-space ICA and power analysis to EEG containing microsleeps so as to detect activity during microsleeps, find the

locations of the sources of such activity, and characterize their time courses via time-frequency analysis.

2. Methods

2.1. Participants

Five right-handed healthy male volunteers, aged 26–38 years (mean = 29.5) with no history of neurological, psychiatric, or sleep disorder, participated in the study. All subjects provided informed consent prior to participating in the study. Ethical approval for the study was obtained from the New Zealand Upper South A Ethics Committee. Subjects were asked not to consume any stimulants or depressants, such as alcohol, caffeine, or nicotine, during the 4 h prior to the session. They were required to keep a detailed diary of their sleep habits and to wear an Actiwatch (Mini Mitter Inc., Bend OR, USA) to measure their sleep-wake activity during the six days and five nights prior to the session. The diary and Actiwatch data were used to verify that the subjects had regular sleep habits in the week prior to the session. A set of questionnaires was used to assess general health, sleep quality, morningness-eveningness, and daytime sleepiness. Subjects were provided with lunch approximately 15 min before the session.

2.2. Apparatus

The participants performed the task in a supine position, during which the tracking task was displayed on the visual system.

The vision system for stimulus presentation used two mirrors mounted on the table above their head to allow participants to see an LCD monitor (Viewsonic 17) displaying the 2D tracking task. A portable eye-video system (iViewXTM HED, SMI, Teltow, Germany) was connected to an iViewXTM video recording system. Eye-video was recorded simultaneously and synchronously with visuomotor response and other physiological recording systems.

A Neuroscan 64-channel 10–10 cap was used for EEG electrode placement and EEG was recorded on a Neuroscan EEG system (Compumedics, Charlotte, NC, USA).

2.3. The 2D tracking task

The tracking task had a continuously moving pseudo-random target which allowed changes in behavior to

be detected with high temporal resolution.³² There were no flat segments in the tracking target, which is important as flat segments in the target motion make it difficult to identify microsleeps. The tracking error was defined as the Euclidean distance between the center of the red response disc and the center of the yellow target disc.

2.4. Experimental paradigm

Subjects took part in the study in early afternoon (commencing between 1:00 pm and 2:00 pm), corresponding with both post-lunch and a low point in the circadian cycle, so as to intentionally be at a time of day coinciding with increased propensity for microsleeps. They had to continuously manoeuvre a finger-based joystick to perform a 2D tracking task. A finger-based joystick (Current Designs, Philadelphia, PA, USA) was placed alongside the supine subject and they held the joystick between the thumb and index fingers of their right hand. Data from the joystick were sampled at 60 Hz and presented as the response disc. Subjects were familiarized with the tracking task and joystick before the start of the session.

2.5. Definition of microsleeps based on tracking task and eye-video

Two types of tracking error were used to identify microsleeps^{8,33}:

- flat tracking, in which the response disc simply stops moving for > 500 ms while the target is moving,
- incoherent tracking, in which the response disc is moving away from target disc for > 500 ms.

A microsleep was defined operationally as:

- flat or incoherent tracking for > 500 ms,
- full or partial eye closure (phasic/transient), and
- drowsy behavior.

Drowsy behavior was defined as the subject appearing subdued, droopy eyes, and often a glassy-eyed appearance.^{8,33}

2.6. EEG data containing microsleeps

There were five sets of EEG data in this study: Subjects 102–106. Subjects carried out the 2D tracking

task in a mock-MRI scanner, during which eye-video was recorded to assist in the identification of microsleeps. Each EEG was 60 min long. The first 10 min was voluntary eye closure, with repeated cycles of 30-s eyes closed and 30-s eyes open while performing the tracking task. During the remaining 50 min, the subjects continuously performed the 2D tracking task.

EEG was sampled at 250 Hz and band-pass filtered at 1.0–45 Hz. The Montreal Neurological Institute (MNI) coordinates³⁴ were used to describe locations in the brain. The boundary element method (BEM)³⁵ model of the head with three layers and a conductivity ratio of skull to soft tissue of 0.0125, obtained from the average MNI-template brain and implemented via the FieldTrip toolbox,³⁶ was used to calculate the lead-field matrix for the minimum-variance beamformer. The EEGLAB toolbox³⁷ was

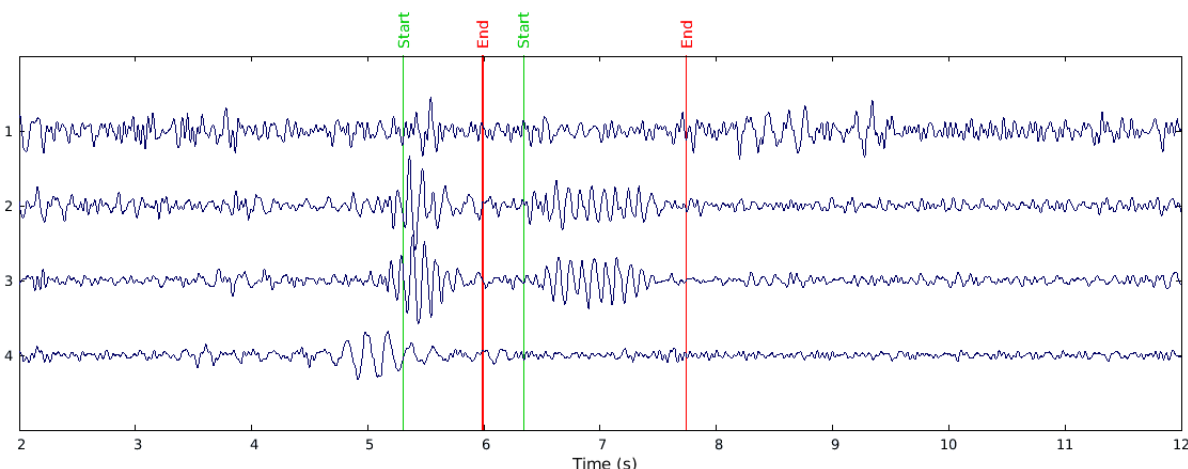
used to carry out ICA of the EEG via the Infomax algorithm.³⁸

2.7. Processing of EEG

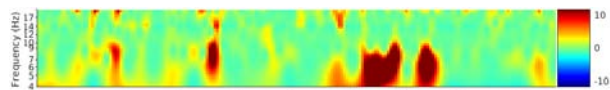
2.7.1. Pre-processing of EEG

Pre-processing included the following steps:

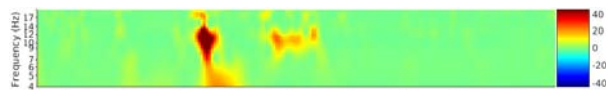
- Visual inspection: All microsleeps were visually inspected to identify any strong artefacts during or close to microsleeps. Microsleeps contaminated with strong artefacts were rejected so that only clean microsleeps remained.
- Eye artefact removal: ICA was applied to the EEG to remove eye movement and eye-blink artefacts. The data set was first split into sets of frequencies above and below 4 Hz. ICA was then applied to the low frequency part of the EEG. Independent components related to artefacts were identified and



(a) Component time courses



(b) ERSP of component 1



(c) ERSP of component 2



(d) ERSP of component 3



(e) ERSP of component 4

Fig. 1. (Color online) (a) Time-courses of components separated by source-space ICA for an EEG epoch from Subject 104 containing 2 microsleeps. The ERSPs of components 1–4 are shown in (b)–(e). The baseline for ERSPs was considered to be 0.5–3.5 s prior to onset of microsleep. Components 1 and 4 were dominated by theta-band activity and components 2 and 3 had alpha-band burst activity time-locked to microsleeps. The green lines in (a) indicate the onsets and the red lines the offsets of the microsleeps.

removed to obtain a clean low frequency EEG data. After artefact removal, the low frequency data set was added back to the high frequency data set.

2.7.2. Source separation of microsleep EEG

As the total microsleep duration for each subject was only a small proportion of the total task duration (e.g. 113s versus ~ 48 min for Subject 106), applying ICA on the full 50 min of EEG would likely result in microsleep activity not being identifiable by way of separate components. Therefore, for each subject, we identified the EEG epochs with multiple microsleeps and applied source-space ICA to each of these epochs to separate the sources, reconstruct the time courses, and localize their origin in the

brain. In source-space ICA,¹² the weight-normalized minimum-variance beamformer²⁵ is first applied to an EEG epoch to project the sensor into source-space via a 3D scanning grid here (10 mm^3). Singular value decomposition (SVD) is then applied to reduce the size of the data matrix and to separate the spatial and temporal subspaces. This is followed by application of ICA to the temporal subspace to identify temporally independent components. Localization of the temporal components is obtained via multiplication of the ICA mixing matrix with the spatial subspace.

2.7.3. Estimating the source maps

In order to obtain localization maps for theta-band components, the components which have activity

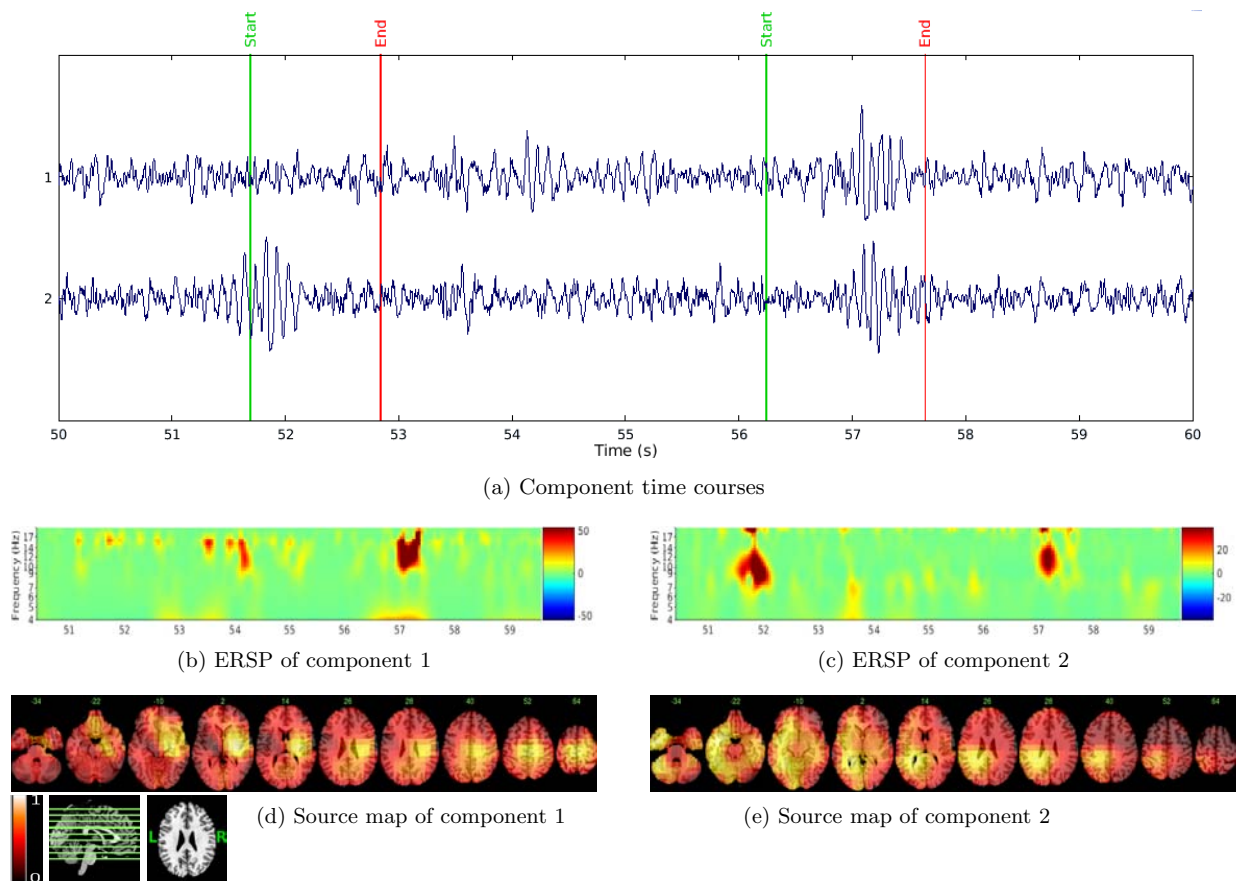


Fig. 2. (Color online) (a) Time courses of two components from Subject 106 with alpha-band burst activity time-locked to microsleeps. The ERSPs of the components are shown in (b) and (c). The baseline for ERSPs was 49–51 s. (d) and (e) show source maps for these two components, obtained via source-space ICA normalized mixing weights. Component 1 shows activity in the right temporal lobe and the posterior cingulate cortex, and bilaterally in motor cortex, whereas component 2 shows an extended area in the left hemisphere including the temporal lobe and posterior cingulate cortex to be the origin of the source. The green lines in (a) indicate the onsets and the red lines the offsets of the microsleeps.

during or close to onset of microsleeps were retained while all other components were rejected. In this way, only the components which contributed to the theta band were present in the source-space signals. To identify which components were time-locked to microsleeps, visual inspection of the component time-series together with event-related spectral perturbation (ERSP) of the components provided a visual and quantitative approach to identify the components. ERSP measures mean event-related changes in the power spectrum for a data channel or component.^{38,39} Subjects usually had two to four alpha-band components time-locked to the microsleeps.

The next step was to measure the power of the source-space for the whole duration of the EEG epoch to produce the source maps for theta-band components. For alpha-band components a slightly different procedure was applied:

- alpha-band components with time-locked activity (i.e. only active during microsleeps) were retained and the remaining components were rejected,
- the power of the source-space was measured over the duration of each microsleep and then normalized,
- normalized power maps of each microsleep were added to each other and normalized again to

obtain a single map for every subject representing the map of the alpha-band components,

- the normalized power maps for each subject were added to each other and normalized to obtain a group map.

The reason for the different approaches to theta-band and alpha-band source reconstruction is that theta-band components had activity prior, during, and after microsleeps. Therefore, we cannot set a specific time window for measuring the theta-band power of source-space. Whereas, the alpha-band components were normally active only during microsleeps, indicating such components are specifically related to the microsleeps. Examples of theta and alpha components are shown in Fig. 1. Components 1 and 4 are dominated by theta activity and components 2 and 3 have alpha-band activity time-locked to the onset of the microsleeps.

Furthermore, some components had more frequent alpha-burst activity compared with the other components during microsleeps. Therefore, measuring power for the duration of microsleeps preserves the contribution of each source to the averaged map of the microsleeps for subjects. An example of this situation is shown in Fig. 2 where component 1 only had burst activity for the second microsleep, whereas

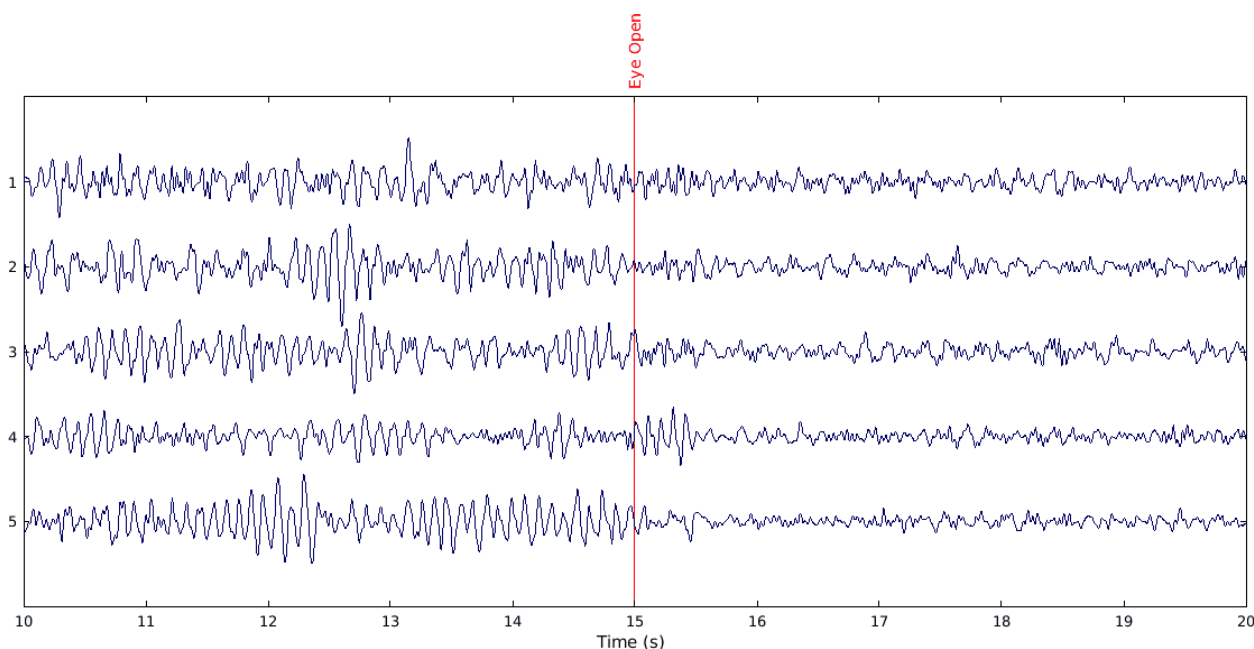


Fig. 3. Time-courses of components separated by source-space ICA for an EEG epoch for Subject 104 containing eye closure. The red line is when the subject opens his eyes.

component 2 had burst activity for both microsleeps. This also indicates that there are several sources associated with microsleeps (sleep spindles) which may or may not fire simultaneously. The source maps for these two components, obtained via source-space ICA mixing weights, show the left and right structure of the two components. Both components had clusters extending bilaterally over the anterior temporal gyri, hippocampi, and posterior cingulate cortex.

2.8. Statistical comparison of sources of microsleeps and voluntary eye closures

To identify sources of alpha during voluntary eye closures, source-space ICA was applied to a 60s epoch of all five subjects with 30s of eye closures and 30s of eyes open. Similar procedures to that for alpha-band components of microsleeps were applied to components time-locked to eye closure to obtain source maps of eye closure alpha activity. By this process, 10 normalized maps from five subjects were obtained: five for microsleep alpha power and five for eye closure alpha power. To identify significant clusters across the 10 maps, spatial-based voxel-wise statistics were performed using a permutation-based inference tool for nonparametric statistical thresholding (using Randomize tool in FSL). The results from this were then compared to the alpha sources identified during microsleeps. An example of the

sources having alpha-band activity due to the voluntary eye closure is shown in Fig. 3.

3. Results

Microsleeps were identified behaviorally in all five subjects (Table 1).

3.1. Individual EEG analysis

Figure 4 shows the individual maps obtained after subtraction of normalized microsleep alpha power maps from normalized eye closure alpha power maps. All subjects show bilateral sources in the temporal lobes and hippocampi, with higher power during microsleeps than voluntary eye closures, with the exceptions of subject 104 whose activity was only on the right side. Also, except for 103, all subjects had higher power in the frontal lobes during voluntary eye closure than microsleeps.

Table 1. Summary of the microsleeps identified behaviorally during the 50 min 2D tracking task.

Subject	Total microsleeps	Artefact-free microsleeps	Average duration
102	25	25	2.3 s
103	45	33	6.2 s
104	6	4	1.0 s
105	10	2	0.9 s
106	43	39	2.1 s

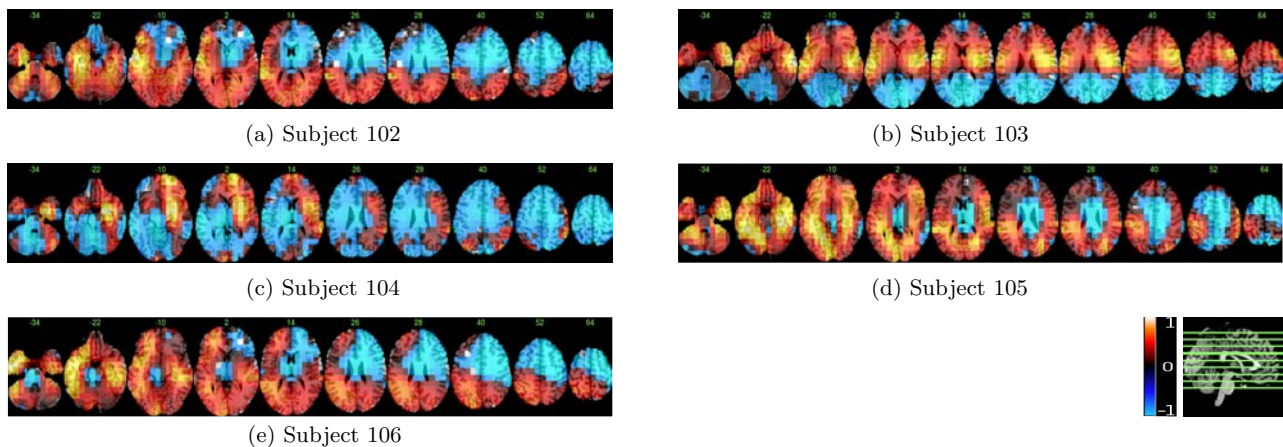


Fig. 4. Source maps of subjects 102–106 obtained after subtraction of the normalized power map of microsleeps alpha-band components from voluntary eye closure alpha-band components. Hot areas indicate higher power during microsleeps relative to voluntary eye closure, whereas cold areas indicate higher activity during voluntary eye closures. All maps were normalized with respect to the maximum absolute value in that map.

As mentioned earlier, the aim of these plots is to differentiate the voluntary eye closure alpha sources from microsleep-related sources. This is important as, in both situations, the subject has his eyes shut. But eye closure during a microsleep occurs approximately around onset of the microsleep and is not voluntary and, unlike voluntary eye closure alpha components which can persist for the duration of

the eye closure, microsleep alpha-band components are short (0.5–3.0s), regardless of the duration of the microsleeps. An example of this can be seen in Subject 103 who had several microsleeps longer than 10s but only 1–2s alpha-burst activity for such long microsleeps. Note that this comparison cannot be applied to the theta-band components of microsleeps, as theta activity is not time-locked

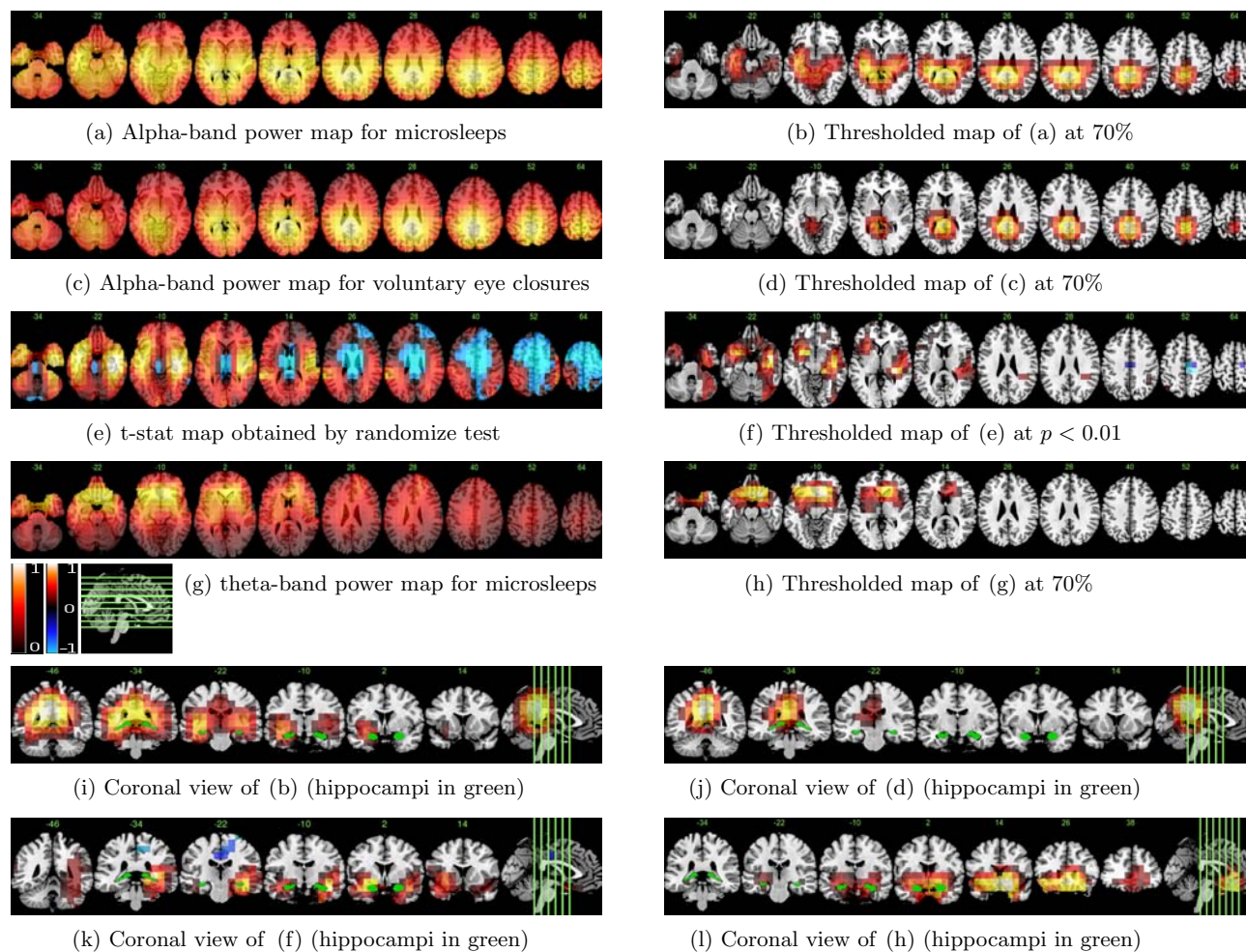


Fig. 5. (Color online) Normalized source power map for group analysis of alpha band for microsleeps (a) and (b), and for group analysis of voluntary eye closures (c) and (d). (b) and (d) are thresholded at 70% of the maximum power. Extended areas including temporal lobes, hippocampi, and posterior cingulate cortex are the sources associated with microsleep alpha bursts, whereas the posterior cingulate cortex is the focal point of the voluntary eye closure alpha power. (e) shows the t -stat map obtained by spatial-based voxel-wise permutation-based inference for nonparametric statistical thresholding of difference between the five maps of microsleep alpha and the five maps of eye closure alpha. (f) is the result of thresholding (e) at $p < 0.01$. This shows a significant increase in alpha-burst activity during microsleeps relative to eye closures in the bilateral anterior temporal lobes and hippocampi, as well as decreased activity in the posterior cingulate cortex. (g) is the normalized group theta-band power map for theta-band components and (i) is (g) thresholded at 70% of the maximum. The bilateral frontal-orbital cortex is the primary source of the theta activity, as well as frontal hippocampi. (i)–(l) are the coronal views of (b), (d), (f), and (h) respectively with the hippocampi highlighted in green.

to the voluntary eye closure. However, the most powerful independent components of EEG segments containing microsleeps were theta-band components with activity which could occur before, during, or after microsleeps, and appear more an indication of drowsiness than microsleeps per se.

3.2. Group results

Group results allow stronger conclusions to be made on the anatomical location of brain sources of neuroelectric activity specific to microsleeps. For this, average tomographic maps of alpha and theta components with strong activity associated with microsleeps were derived.

Figure 5(a) shows the normalized group power map of alpha-band components for the microsleeps from five subjects, and Fig. 5(b) shows the same map thresholded at 70% of the maximum. Based on Fig. 5(b), the sources associated with microsleep alpha are bilateral posterior cingulate cortex, hippocampi, and anterior temporal gyri.

Figure 5(c) shows the normalized group power map of alpha-band components for the voluntary eye-closure from five subjects, and Fig. 5(d) shows the same map thresholded at 70% of the maximum. The sources associated with voluntary eye closure alpha are originated from posterior cingulate cortex (Fig. 5(d)).

Figure 5(e) shows the *t*-stat map obtained after spatial-based voxel-wise statistics using a permutation-based inference tool for nonparametric statistical thresholding (using Randomise tool in FSL) on the 10 maps of the five subjects (five for microsleep alpha and five for voluntary eye closure alpha). Figure 5(f) shows the same map thresholded at $p < 0.01$. Significant activity was observed in the anterior temporal lobe (superior and inferior) and the hippocampi during microsleep alpha bursts compared to voluntary eye closures. Conversely, greater activity due to voluntary eye closure was observed in the posterior cingulate cortex.

Figure 5(g) shows the group power map of theta-band components for the EEG segments containing microsleeps from the five subjects, and Fig. 5(h) shows the same map thresholded at 70% of the maximum. The origin of the theta sources is bilaterally in the frontal orbital area and frontal hippocampi as shown in Fig. 5(i).

Figures 5(i)–5(l) show the coronal view of Figs. 5(b), 5(d), 5(f), and 5(h) respectively, with hippocampi highlighted in green.

4. Discussion

Our study is the first to have shown that microsleeps are often associated with alpha spindles corresponding to Stage-2 sleep spindles. Furthermore, we have shown that these spindles originate from a network comprising the bilateral anterior temporal lobes and hippocampi.

In all five subjects, source-space ICA revealed 2–4 components time-locked to microsleeps with alpha burst activity. However, not all components had burst activity during every microsleep. As was shown in Fig. 2(a), such components had burst activities independent from each other, indicating several underlying sources associated with alpha-burst activity of microsleeps. This was also shown in terms of anatomical location of such sources (Figs. 2(a) and 5(b)). Similarly, there were 3–5 alpha-band components time-locked to the voluntary eye closures but these all had their sources in the bilateral posterior cingulate cortex.

Considering the location and shape of the microsleep-alpha components separated by source-space ICA, and the behavioral correlates of microsleeps, it seems clear that the microsleep alpha components are sleep spindles. In human EEG, sleep spindles are grouped in short 0.5–3.0s periods of 11–15Hz oscillations, forming a waxing and waning envelope, that recurs periodically every 5–15s and typically appear during the light stage of slow-wave sleep (Stage 2).⁴⁰ Source localization via dipole modeling for MEG sleep spindles and alpha activity shows that spindles originate from pre- and post-central cortical areas whereas the alpha rhythm originates from posterior regions.⁴¹ The cortical representations of these have also been shown to be different.⁴¹

A recent fMRI study⁴² of EEG sleep spindles showed increased signal in the thalamus, posterior cingulate, right precuneus, putamen, paracentral cortex, and temporal lobes. This contrasts with our fMRI study in which we found a substantial bilateral decrease in activity in the thalamus and posterior cingulate cortex during microsleeps.⁸ It also contrasts with the current study which found microsleep

alpha spindles to be, at least primarily, generated strongly in the anterior temporal lobes and hippocampi. We are unable to explain this difference other than to conjecture that sleep spindles generated during extended Stage-2 normal sleep as opposed to microsleeps going transiently into and out of light Stage-2 sleep have different patterns of activation. This difference is perhaps not surprising when microsleeps clearly have, at least in part, different underlying mechanisms from normal Stage-2 sleep in that microsleeps during an active task (i) are involuntary and undesired and (ii) reflect a ‘consequences’ region in the brain which is able to pull a person out of a microsleep after a few seconds (even though this is sometimes too late), despite the brain’s need and drive for a fatigue/sleep break.

Another study⁴³ used simultaneous recording of intracerebral EEG from hippocampal and several distributed neocortical sites in neurosurgical patients to show that sleep spindles consistently appear in the hippocampus several minutes before the onset of sleep.

Two studies^{44,45} divided sleep spindles into slow spindles (11–13 Hz) and fast spindles (13–15 Hz) and found both the hippocampi and thalami to be activated during sleep spindles. Conversely, another study⁴³ found no activity in the hippocampi during spindles but instead found that the hippocampus functional connectivity map overlaps highly with the sleep-spindle activation map.

Another study⁴⁶ found alpha spindles to be an indication of prolonged brake reaction time when driving with an auditory secondary task compared to only driving. They concluded that alpha spindles are an indication of reduced visual processing due to internalization of attention caused by auditory distraction.

Similar to the alpha band, there were one or two theta components separated by source-space ICA which had strong activity in the vicinity of microsleeps. These theta-band components were mostly found to come from the frontal orbital cortex area. In humans, EEG power in the theta band during quiet waking increases during sleep deprivation, and predicts a subsequent homeostatic increase of slow-wave activity during sleep.⁴⁷ Theta-burst activity has also been reported to be related to microsleeps.⁶ Our signal processing approach and

results could be used to improve the performance of automated sleep-detection/staging systems^{48,49} by providing new features to sleep classification/rating algorithms based upon theta and alpha burst activity. Features indicating theta and alpha bursts can be derived from real-time beamformer reconstruction of activity from the frontal orbital cortex and the hippocampi, respectively. The source-space ICA algorithm,^{12,50} used here for reconstruction of microsleep-related sources, could also be used for reconstruction of sources of interictal or seizure epileptic activity and also used to identify new features in source-space for incorporating in detection algorithms.⁵¹

5. Limitations

The findings of the current study need to be considered in the light of some limitations. We used 64-channel EEG whereas higher density EEG (e.g. 128 channels) would likely increase accuracy of source localization. The head models used in the beamforming were based on the standard MNI model rather than individual MRI of subjects. The number of subjects and events (i.e. five subjects and 103 microsleeps) in our study were relatively small; notwithstanding, similar numbers have successfully been used in other studies of sleep spindles (e.g. seven subjects and 106 spindles⁴¹). Furthermore, we focused on the alpha and theta bands only, whereas, using intracellular recordings, frequencies of below 1 Hz have been also shown to be associated with sleep spindles and early stages of sleep.⁵²

6. Conclusion

In this study, microsleep-related activities in the EEG were detected, characterized, separated from eye closure-related activity, and source-localized in the brain. Theta-related activity was identified as originating bilaterally from the frontal-orbital cortex. Alpha-band burst activity was seen to originate bilaterally from the anterior temporal lobes and hippocampi. The microsleep-related alpha activity was similar to that of sleep spindles in terms of frequency and amplitude-profile, indicating that at least a substantial proportion of microsleeps are equivalent to brief instances of Stage-2 sleep.

References

1. M. T. R. Peiris, R. D. Jones, P. R. Davidson, G. J. Carroll and P. J. Bones, Frequent lapses of responsiveness during an extended visuomotor tracking task in non-sleep-deprived subjects, *J. Sleep Res.* **15** (2006) 291–300.
2. T. Akerstedt, I. Torsvall and M. Gillberg, Sleepiness in shiftwork, a review with emphasis on continuous monitoring of EEG and EOG, *Chronobiol. Int.* **4** (1987) 129–140.
3. M. Congedo, F. Lotte and A. Lecuyer, Classification of movement intention by spatially filtered electromagnetic inverse solutions, *Phys. Med. Biol.* **51** (2006) 1971–1989.
4. J. McLaren, J. C. Erie and R. F. Brubaker, Computerized analysis of pupillograms in studies of alertness, *Invest. Ophthalmol. Vis. Sci.* **33** (1992) 671–676.
5. D. Sommer, M. Golz, T. Schnupp, J. Krajewski, U. Trutschel and D. Edwards, A measure of strong driver fatigue, in *Proc. Int. Driv. Symp. Human Fact. Driv. Assess. Train. Vehicle Desi.*, Vol. 5 (2009), pp. 9–15.
6. D. Sommer, T. Hink and M. Golz, Application of learning vector quantization to detect drivers dozing-off, *Eur. Symp. Intel. Technol. Hybrid Syst. Implement. Smart Adapt. Sys.*, Vol. 2 (2002), pp. 275–279.
7. J. L. Ong, D. Kong, T. T. Y. Chia, J. Tandhi, B. T. T. Yeo and M. W. L. Chee, Co-activated yet disconnected neural correlates of eye closures when trying to stay awake, *Neuroimage* **118** (2015) 553–562.
8. G. R. Poudel, C. R. H. Innes, R. Watts, P. Bones and R. D. Jones, Losing the struggle to stay awake: Divergent thalamic and cortical activity during behavioral microsleeps, *Hum. Brain Mapp.* **35** (2014) 257–269.
9. J. Toppi, L. Astolfi, G. R. Poudel, C. R. Innes, F. Babiloni and R. D. Jones, Time-varying effective connectivity of the cortical neuroelectric activity associated with behavioral microsleeps, *Neuroimage* **124** (2016) 421–432.
10. Y. Aoki, R. Ishii, R. D. Pascual-Marqui, L. Canuet, S. Ikeda, M. Hata *et al.*, Detection of EEG-resting state independent networks by eLORETA-ICA method, *Front. Hum. Neurosci.* **9** (2015) 1–12.
11. Y. Jonmohamadi, G. Poudel, C. Innes and R. Jones, Voxel-ICA for reconstruction of source signal time-series and orientation in EEG and MEG, *Australas. Phys. Eng. Sci. Med.* **37** (2014) 457–464.
12. Y. Jonmohamadi, G. Poudel, C. Innes and R. Jones, Source-space ICA for EEG source separation, localization, and time-course reconstruction, *Neuroimage* **101** (2014) 720–737.
13. F. de Pasquale, S. Della Penna, A. Z. Snyder, C. Lewis, D. Mantini *et al.*, Temporal dynamics of spontaneous MEG activity in brain networks, *Proc. Natl. Acad. Sci. U.S.A.* **107** (2009) 6040–6045.
14. M. J. Brookes, M. Woolrich, H. Luckhoo, D. Price, J. R. Hale, M. C. Stephenson *et al.*, Investigating the electrophysiological basis of resting state networks using magnetoencephalography, *Proc. Natl. Acad. Sci. U.S.A.* **108** (2011) 16783–16788.
15. H. Luckhoo, J. R. Hale, M. G. Stokes, A. C. Nobre, P. G. Morris *et al.*, Inferring task-related networks using independent component analysis in magnetoencephalography, *Neuroimage* **62** (2012) 530–541.
16. J. M. Stephen, B. A. Coffman, R. E. Jung, J. R. Bustillo, C. J. Aine *et al.*, Using joint ICA to link function and structure using MEG and DTI in schizophrenia, *Neuroimage* **83** (2013) 418–430.
17. J. C. Mosher, P. S. Lewis and R. M. Leahy, Multiple dipole modeling and localization from spatio-temporal MEG data, *IEEE Trans. Biomed. Eng.* **39** (1992) 541–557.
18. J. Sarvas, Basic mathematical and electromagnetic concepts of the biomagnetic inverse problem, *Phys. Med. Biol.* **32** (1987) 11–22.
19. K. Uutela, M. S. Hämäläinen and R. Salmelin, Global optimization in the localization of neuromagnetic sources, *IEEE Trans. Biomed. Eng.* **45** (1983) 716–723.
20. M. S. Hämäläinen and R. J. Ilmoniemi, Interpreting magnetic fields of the brain: Minimum norm estimates, *Med. Biol. Eng. Comput.* **32** (1994) 35–42.
21. A. M. Dale, A. K. Liu, B. R. Fischl, R. L. Buckner, J. W. Belliveau, J. D. Lewine *et al.*, Dynamic statistical parametric mapping: Combining fMRI and MEG for high-resolution imaging of cortical activity, *Neuron* **26** (2000) 55–67.
22. R. D. Pascual-Marqui, Standardized low-resolution brain electromagnetic tomography (sLORETA): Technical details, *Methods Find. Exp. Clin. Pharmacol.* **24** (Suppl D) (2002) 5–12.
23. R. E. Greenblatt, A. Ossadtchi and M. E. Pflieger, Local linear estimators for the linear bioelectromagnetic inverse problem, *IEEE Trans. Biomed. Eng.* **53** (2005) 3403–3412.
24. S. E. Robinson and J. Vrba, *Functional Neuroimaging by Synthetic Aperture Magnetometry (SAM)*, in *Proc. 11th Int. Conf. Biomagnetism* (Tohoku Univ. Press: Sendai, 1998), pp. 302–305.
25. K. Sekihara, S. S. Nagarajan, D. Poeppel, A. Marantz and Y. Miyashita, Reconstructing spatio-temporal activities of neural sources using an MEG vector beamformer technique, *IEEE Trans. Biomed. Eng.* **48** (2001) 760–771.
26. B. D. Van Veen, W. van Drongelen, M. Yuchtman and A. Suzuki, Localization of brain electrical activity via linearly constrained minimum variance spatial filtering, *IEEE Trans. Biomed. Eng.* **44** (1997) 867–880.
27. Y. Jonmohamadi, C. Innes, G. Poudel, D. Weiss, R. Krueger *et al.*, Comparison of beamformers for EEG

- source signal reconstruction, *Biomed. Signal Process. Control* **14** (2014) 175–188.
28. K. Sekihara and S. S. Nagarajan, *Adaptive Spatial Filters for Electromagnetic Brain Imaging* (Springer, Berlin, 2008).
 29. S. Sanei and J. A. Chambers, *EEG Signal Processing* (John Wiley & Sons, Ltd, Chichester, West Sussex, 2007).
 30. S. Makeig, S. Debener, J. Onton and A. Delorme, Mining event-related brain dynamics, *Trends Cogn. Sci.* **8** (2004) 204–210.
 31. E. M. Ventouras, P. Y. Ktonas, H. Tsekou, T. Paparrigopoulos, I. Kalatzis and C. R. Soldatos, Independent component analysis for source localization of EEG sleep spindle components, *Comput. Intell. Neurosci.* **2010** (2010) 1–12.
 32. G. R. Poudel, R. D. Jones and C. R. H. Innes, A 2D pursuit tracking task for behavioural detection of lapses, *Australas. Phys. Eng. Sci. Med.* **31** (2008) 528–529.
 33. C. Innes, G. Poudel and R. Jones, Efficient and regular patterns of nighttime sleep are related to increased vulnerability to microsleeps following a single night of sleep restriction, *Chronobiol. Int.* **30** (2013) 1187–1196.
 34. G. Bush and P. Luu, Cognitive and emotional influences in anterior cingulate cortex, *Trends Cogn. Sci.* **4** (2000) 215–222.
 35. T. F. Oostendorp and A. van Oosterom, Source parameter estimation in inhomogeneous volume conductors of arbitrary shape, *IEEE Trans. Biomed. Eng.* **36** (1989) 382–391.
 36. R. Oostenveld, P. Fries, E. Maris and J. M. Schoffelen, FieldTrip: Open source software for advanced analysis of MEG, EEG, and invasive electrophysiological data, *Comput. Intell. Neurosci.* **2011** (2011) 1–9.
 37. A. Delorme and S. Makeig, EEGLAB: An open source toolbox for analysis of single-trial EEG dynamics, *J. Neurosci. Methods* **134** (2004) 9–21.
 38. A. J. Bell and T. J. Sejnowski, An information-maximization approach to blind separation and blind deconvolution, *Neural Comput.* **7** (1995) 1129–59.
 39. S. Makeig and M. Inlow, Lapses in alertness: Coherence of fluctuations in performance and EEG spectrum, *Electroencephal. Clin. Neurophysiol.* **86** (1993) 23–35.
 40. M. Bonjean, T. Baker, M. Lemieux, T. Timofeev, I. Sejnowski and M. Bazhenov, Corticothalamic feedback controls sleep spindle duration *in vivo*, *J. Neurosci.* **25** (2011) 9124–9134.
 41. I. Manshanden, J. C. De Munck, N. R. Simon and F. H. Lopes da Silva, Source localization of MEG sleep spindles and the relation to sources of alpha band rhythms, *Clin. Neurophysiol.* **12** (2002) 1937–1947.
 42. M. Caporro, Z. Haneef, H. J. Yeh, A. Lenartowicz, C. Buttinelli, J. Parvizi et al., Functional MRI of sleep spindles and K-complexes, *Clin. Neurophysiol.* **2** (2012) 303–309.
 43. S. Sarasso, P. Proserpio, F. Moroni, M. Ferrara, A. M. M. De Gennaro, L. Pigorini et al., Hippocampal sleep spindles preceding neocortical sleep onset in humans, *Neuroimage* **86** (2014) 425–32.
 44. K. C. Andrade, V. I. Spoomaker, M. Dresler, R. Wehrle, F. Holsboer, P. G. Sämann and M. Czisch, Sleep spindles and hippocampal functional connectivity in human NREM sleep, *J. Neurosci.* **31** (2011) 10331–10339.
 45. M. Schabus, T. T. Dang-Vu, G. Albouy, E. Balteau, M. Boly et al., Hemodynamic cerebral correlates of sleep spindles during human non-rapid eye movement sleep, *Proc. Natl. Acad. Sci. USA.* **104** (2007) 13164–13169.
 46. A. Sonnleitner, M. Sebastian, T. Michael Simon, S. Willmann, A. Ewald, A. Buchner et al., EEG alpha spindles and prolonged brake reaction times during auditory distraction in an on-road driving study, *Accid. Anal. Prev.* **62** (2014) 110–118.
 47. V. V. Vyazovskiy and I. Tobler, Theta activity in the waking EEG is a marker of sleep propensity in the rat, *Brain Res.* **1050** (2005) 64–71.
 48. H. Wang, C. Zhang, T. Shi, F. Wang and S. Ma, Real-time EEG-based detection of fatigue driving danger for accident prediction, *Int. J. Neural. Syst.* **25** (2015) 1550002.
 49. U. R. Acharya, S. Bhat, O. Faust, H. Adeli, E. C. Chua, W. J. Lim and J. E. Koh, Nonlinear dynamics measure for automated EEG-based sleep stage detection, *Eur. Neurol.* **74** (2015) 268–287.
 50. Y. Jonmohamadi and R. Jones, Source-space ICA for MEG source imaging, *J. Neurol. Eng.* **13** (2016) 016005.
 51. S. Ghosh-Dastidar, H. Adeli and N. Dadmehr, Principal component analysis-enhanced cosine radial basis function neural network for robust epilepsy and seizure detection, *IEEE Trans. Biomed. Eng.* **55** (2008) 512–518.
 52. A. Destexhe, S. W. Hughes, M. Rudolph and V. Crunelli, Are corticothalamic ‘up’ states fragments of wakefulness? *Trends Neurosci.* **30** (2007) 334–342.